shown in Figure 12. Moreover, the BMDs of vertebral bone of the D10 and D20 groups were significantly lower than that of the N10 group. These results suggest that the Zn–TCP injection improved the systemic BMD, but the effect was not sufficient to increase the BMD of the diseased rats to the levels of the N10 group. In contrast, BMDs of the femurs were measured to evaluate the local therapeutic effect of Zn–TCP injection on the diseased rats by comparing the BMD between the injected side and noninjected side. According to the rank order of BMD (Fig. 11), BMDs of the D10L and D20L were significantly higher than that of the D0L, and also those of the D10R and D20R, respectively. This suggests that the Zn–TCP injections improved the BMD of the femur on the injected side more than on the noninjected side. There was no significant difference in femoral BMD between the D20L and N10 groups, and between the D10R and N10 groups. Therefore, the Zn–TCP injections were pharmacologically effective in improving the systemic BMD, and the local effect on the femora was more pronounced than the systemic effect.

After Zn–TCP injections, macroscopic examination revealed no inflammatory reaction and no Zn–TCP particles in the injected sites. This indicates that the Zn–TCP particles have excellent biocompatibility. In addition, the rats injected with Zn–TCP appeared healthier, and retained more normal fur than the diseased rats.

CONCLUSION

Zn-AUC, ALP-AUC, body weight, and BMD of the femora and lumbar vertebra of the D10 and D20 groups injected with 10 and 20 mol % Zn–TCP suspensions were all higher than those in animals injected with Zn-free TCP. The results indicate that long-term sustained Zn release from Zn–TCP may improve bone mineral density in Zn-deficient osteoporotic rats. Based on these *in vivo* results, we conclude that the Zn–TCP suspension injections were adequate to viably sustain Zn release for more than 1 week.

References

1. Williams RJP. Zinc: What is its role in biology? Endeavour 1984;8:65–70.
2. Kishi S, Yamaguchi M. Inhibitory effect of zinc compounds on osteoblast-like cell formation in mouse marrow cultures. Biochem Pharmacol 1994;48:1225–1230.
3. Szathmari M, Steczek K, Szucs J, Hollo I. Zinc excretion in osteoporotic women. Orv Hetil 1993;134:911–914.
4. Relea P, Revilla M, Pipoll E, Arribas I, Villa LF, Rico H. Zinc, biochemical markers of nutrition, and type I osteoporosis. Age Aging 1995;24:303–307.
5. Ito A, Naito H, Ichinose N, Tateish T. Preparation, solubility and cytocompatibility of zinc-releasing calcium phosphate ceramics. J Biomed Mater Res 2000;50:178–183.
6. Kawamura H, Ito A, Miyakawa S, Layrolle P, Ojima K, Naito H, Ichinose N, Tateish T. Stimulatory effect of zinc on bone formation around zinc-releasing calcium phosphate ceramics implanted rabbits femora. J Biomed Mater Res 2000;50:184–190.
7. Otsuka M, Marunaka S, Matsuda Y, Ito A, Layrolle P, Naito H, Ichinose N. Calcium level-responsive in-vitro zinc release from zinc containing tricalcium phosphate (Zn-TCP). J Biomed Mater Res 2000;52:819–824.
8. Otsuka M, Matsuda Y, Suwa Y, Fox JL, Higuchi WI. A novel skeletal drug delivery system using self-setting calcium phosphate cement 9: Effects of the mixing solution volume on anti-cancer drug release from homogeneous drug-loaded cement. J Pharm Sci 1995;84:733–736.
9. Otsuka M, Nakahigashi Y, Matsuda Y, Fox JL, Higuchi WI, Sugiyama Y. A novel skeletal drug delivery system using self-setting calcium phosphate cement VIII: The relationship between in vitro and in vivo drug release from indomethacin containing cement. J Controlled Release 1997;43:115–122.
10. Otsuka M, Yoneoka K, Matsuda Y, Fox JL, Higuchi WI, Sugiyama Y. Oestradiol release from self-setting apatitic bone cement responsive to plasma-calcium level in ovariectomized rats, and its physicochemical mechanism. J Pharm Pharmacol 1997;49:1182–1188.
11. Kitano M, Ueda J. Calcium spectrophotometrical determination by the methylxyenol blue formed a complex. Nippon Kagaku Kaishi 1971;92:168–170.
12. Yamaguchi M, Kishi S. Prolonged administration of b-alanyl-L-histidinato zinc prevents bone loss in ovariectomized rats. Jpn J Pharmacol 1993;63:203–207.
13. Suda T, DeLuca HF, Tanaka Y. Biological activity of 25-hydroxyergocalciferol in rats. J Nutr 1970;100:1049–1052.
14. Kind PRN, King EJ. Measurement of alkaline phosphatase. J Clin Pathol 1954;7:322–326.
15. Okano T, Kimura N, Tsugawa Y, Okamura Y, Kobayashi T. Roles of parathyroid hormone and 1a,25-dihydroxyvitamin D3 in bone growth of growing male and female rats. J Bone Miner Met 1994;suppl:S23–S26.

Available online at www.sciencedirect.com

SCIENCE DIRECT®

Solid State Ionics 172 (2004) 451–453

SOLID STATE IONICS

www.elsevier.com/locate/ssi

Effect of temperature and kneading solution on polymorphic transformation of mefenamic acid during granulation

Makoto Otsuka*, Fumie Kato, Yoshihisa Matsuda

Department of Pharmaceutical Technology, Kobe Pharmaceutical University, Motoyamakitamachi 4-19-1, Higashi-Nada, Kobe 658-8558, Japan

Received 9 November 2003; received in revised form 4 March 2004; accepted 5 March 2004

Abstract

Form II, mefenamic acid (MA) transformed into form I in various solvents at 25, 33 or 37 °C during kneading, and the transformation rate was dependent on the experimental conditions. The transformation rate of form II measured by X-ray diffraction method increased with increase of temperature and content of ethanol. The kinetic process of form II followed three-dimensional growth of nuclei equation, and the transformation rate constant, k, and induction period, IP, were estimated based on the equation. The k of form II decreased with decrease of temperature, but the IP increased. The transformation rate of form II in ethanol was the fastest, and that in distilled water was the lowest, it was dependent on the solubility of MA in the solution. On the other hand, the k of phase transformation added 1% form I crystals as seeds was much larger than that without seeds, but the IP significantly decreased by seed addition. The result suggested that IP was a nucleus formation process, but the seed addition did not affect the crystal growth process.

Keywords: Solid-state transformation; Polymorph; Mefenamic acid; Kneading; Pharmaceutical process

1. Introduction

Since the polymorphic content of pharmaceuticals was affected on the pharmaceutical properties of the preparations, such as dissolution rate and bioavailability, characterization of the bulk solid powder is very important for drug design of pharmaceuticals. Therefore, many preformulation investigators are currently interested in the monitoring of physicochemical and pharmaceutical properties of pharmaceutical preparations during manufacturing processes in pharmaceutical industry as process analysis technology (PAT).

In the present study, in order to clarify polymorphic transformation during pharmaceutical preparation processes, the effects of temperatures and kneading solution on the polymorphic transformation kinetics of the bulk powder of mefenamic acid (MA) were investigated by thermal analysis and X-ray diffraction analysis as a basic research of PAT. MA which is reported to be in two kinds of polymorphic forms, forms I and II, was used as a model drug; form II had 50% higher solubility in distilled water than form I, so those forms were used as a model drug of PAT research.

2. Experimental section

2.1. Materials

Two kinds of pure polymorphic forms of MA, forms I and II, were prepared by recrystallization in acetone and *N,N*-dimethylformamide, respectively, based on the reported method [1].

2.2. Crystalline transformation process

The sample powders were mixed with kneading solution (distilled water, ethanol or 50% ethanol) at 60 rpm, 25, 33 and 37 °C, respectively. The small amount of sample suspension was collected at suitable intervals and then immediately filtered and dried.

2.3. Analytical method

The physicochemical properties of sample powders were evaluated by using powder X-ray diffraction analysis,

* Corresponding author. Tel.: +81-78-441-7531; fax: +81-78-441-7532.

E-mail address: m-otsuka@kobepharma-u.ac.jp (M. Otsuka).

0167-2738/$ - see front matter © 2004 Published by Elsevier B.V.
doi:10.1016/j.ssi.2004.03.030

differential scanning calorimeter and scanning electron microscopy, respectively.

3. Results and discussion

3.1. Polymorphism of MA

The pure polymorphic form of MA, form I, showed an exothermic peak at 170 °C continuously an endothermic peak due to melt at 231 °C on DSC curves, but form II showed only a melting peak at 233 °C. Both forms showed specific X-ray diffraction profiles, respectively, as reported previously. Romero et al. reported that form II was more soluble than form I, and the solubility changed during the dissolution experiment.

3.2. Polymorphic transformation of MA during granulation process

Form I was stable after kneading with distilled water, ethanol or 50% ethanol at 25, 33 or 37 °C, respectively. Fig. 1 showed changes of X-ray diffraction profiles of form II in distilled water at 25 °C. The kneading results indicated that form II was unstable and transformed into form I in water.

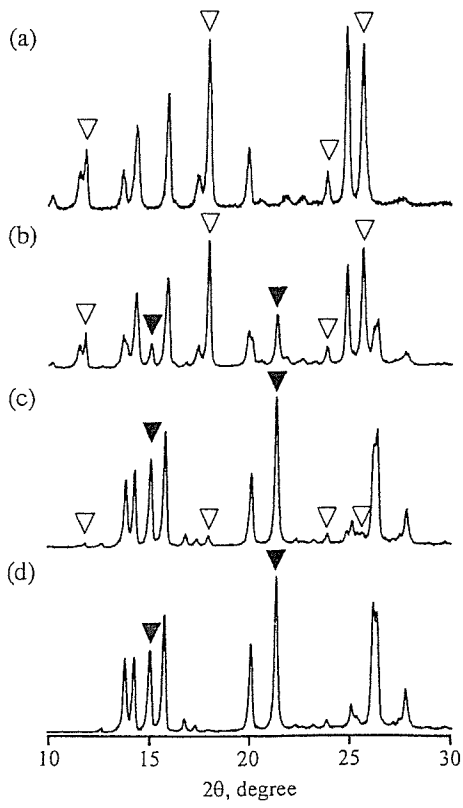

Fig. 1. Powder X-ray diffraction patterns of form II after being suspended in water at 28 °C (a) 0 h; (b) 192 h; (c) 312 h; (d) 456 h. Open and closed triangles represent the significant peaks due to form I and form II, respectively.

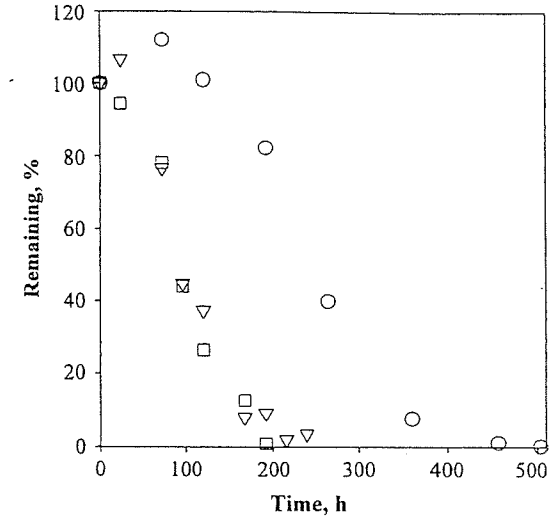

Fig. 2. Percent remaining of form II after being suspended in water. Circles, triangles and squares represent temperature, 28, 33 and 37 °C, respectively.

The results of form II kneading with various solvents at 25, 33 or 37 °C indicated that the transformation rate was dependent on the experimental conditions as shown in Fig. 2.

The transformed polymorphic amount of form II to form I was evaluated based on the specific diffraction peak area (closed triangle in Fig. 1, 2q=11.8, 17.9, 23.8 and 25.6 °) due to transformation on X-ray diffraction profiles. The results of transformation of form II in various solvents at different temperatures suggested that transformation rate of form II increased with increase of temperature and content of ethanol. The transformation kinetics of those processes were evaluated based on 10 kinds of solid-state reaction model equations. Since three-dimensional Avrami (A3) plots for transformation process of form II showed a straight line as shown in Fig. 3, the kinetic process of form II to form I followed three-dimensional growth of nuclei equation, and the transformation rate constant, k, and induction

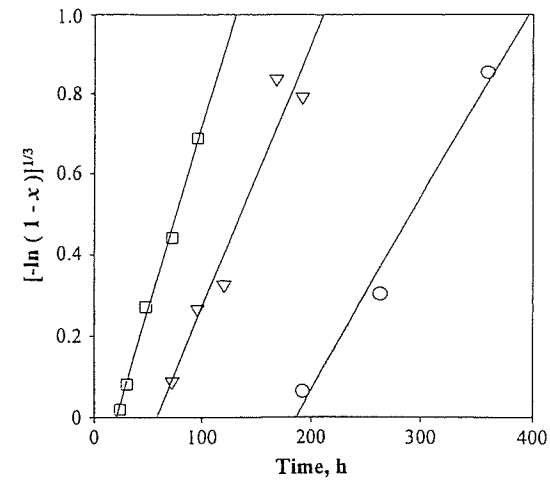

Fig. 3. Dependence of the function $g(x)$ on time for the content of form II suspended in water. Circles, triangles and squares represent temperature, 28, 33 and 37 °C, respectively. A3=$[-\ln(1-x)]^{1/3}$.

Table 1
Rate constants for nucleation formation process of form II and form II + 1% form I crystals

Temperature (°C)	Nuclei formation process (h^{-1})					
	Form II			Form II + I		
	Water	Water–ethanol	Ethanol	Water	Water–ethanol	Ethanol
28	5.37×10^{-3}	5.66×10^{-1}	5.66×10	2.85×10^{-2}	1.68	7.31×10
33	1.71×10^{-2}	2.48×10^{-1}	4.35×10	4.75×10^{-2}	3.99	3.08×10^{2}
37	4.76×10^{-2}	2.71×10^{-1}	6.87×10	7.55×10^{-2}	4.10	1.33×10^{2}

Table 2
Rate constants for growth of nuclei process of form II and form II + 1% form I crystals

Temperature (°C)	Nuclei growth process (h^{-1})					
	Form II			Form II + I		
	Water	Water–ethanol	Ethanol	Water	Water–ethanol	Ethanol
28	4.76×10^{-3}	2.13×10^{-1}	6.03×10^{-1}	5.76×10^{-3}	4.58×10^{-1}	7.44
33	6.51×10^{-3}	4.52×10^{-1}	4.51	8.84×10^{-3}	6.69×10^{-1}	7.27
37	9.10×10^{-3}	4.99×10^{-1}	5.15	1.58×10^{-2}	1.07	1.40×10

period, IP, were estimated based on straight line by the least-squares method. The nuclei formation rate (k_{ip}) was evaluated as reciprocal of the IP. The kinetic parameters of the polymorphic transformation processes were summarized in Tables 1 and 2. The k and k_{ip} of form II decreased with decrease of temperature. The transformation was divided to nuclei formation and nuclei growth processes, the former was related with the IP, and the latter was the slope of the line in Fig. 3.

The transformation rate of form II in ethanol was the fastest, and that in distilled water was the lowest; it was dependent on the solubility of MA in the solution [2]. The result suggested that the transformation performed in the solvent. On the other hand, the k of phase transformation added 1% form I crystals as seed was larger than that without seeds, but the IP significantly decreased by seed addition. The result suggested that IP was a nucleus formation process, but the seed addition did not affect the crystal growth process. Since the transformation process was followed A3 equation, it seemed that the both of nuclei formation and nuclei growth processes were affected by the addition of seed crystals.

4. Conclusion

The results indicated that polymorphic form of MA transformed into stable form during pharmaceutical manufacturing processes. The crystalline transformation induced variability of pharmaceutical properties of final products; especially minor compartment of stable form seed acetated the whole transformation rate.

References

[1] A.J. Aguiar, J.E. Zelmer, J. Pharm.Sci. 58 (1969) 983–987.
[2] S. Romero, et al., Int. J. Pharm. 178 (1999) 193–202.

Evaluation of Titanium Dioxide as a Pharmaceutical Excipient for Preformulation of a Photo-Labile Drug: Effect of Physicochemical Properties on the Photostability of Solid-State Nisoldipine

Koichi KAKINOKI,[a] Kenji YAMANE,[a] Miho IGARASHI,[b] Manami YAMAMOTO,[b] Reiko TERAOKA,[b] and Yoshihisa MATSUDA[b]

[a] *Formulation & Industrial Technology Lab., Taiho Pharmaceutical Co., Ltd.; Tokushima 771–0194, Japan: and* [b] *Department of Pharmaceutical Technology, Kobe Pharmaceutical University; Higashinada-ku, Kobe 658–8558, Japan.*
Received March 11, 2005; accepted April 17, 2005; published online April 27, 2005

To characterize the photocatalytic activity of TiO_2 *via* solid-state reaction, the relationship between the physicochemical properties and photocatalytic activity of TiO_2 was investigated and estimated from the results of photodegradation of nisoldipine. The photodegradation of nisoldipine was significantly enhanced by addition of TiO_2. Two degradation products, nitroso-phenylpyridine derivative and nitro-phenylpyridine derivative, were formed. The degree of photocatalytic activity of TiO_2 was quite different between the various types of TiO_2 investigated, even when the crystalline phase was the same. As a result of the investigations into the relationship between the photocatalytic activity and physicochemical properties of TiO_2, it was found that for the rutile form the photocatalytic activity has good correlation with specific surface area of TiO_2, but poor correlation with water loss on drying of TiO_2. However, for the anatase form, the photocatalytic activity has good correlation with water loss on drying of TiO_2, but poor correlation with specific surface area. Moreover, it was found that the crystallinity of TiO_2 has a moderate correlation with the photocatalytic activity of both crystal forms of TiO_2. These results suggest that a degree of photocatalytic activity of TiO_2 depends on the various physicochemical properties of each type of TiO_2 investigated.

Key words preformulation; solid-state stability; photostability; titanium dioxide; photocatalytic activity

Recently, many studies have been performed on titanium dioxide (TiO_2), which is known as a strong photocatalyst.[1—4] It is one type of inorganic pigment used in a wide range of industrial fields. It has also been used for solid pharmaceutical products as a coating material and its purity has been strictly regulated. According to Japanese Pharmacopoeia XIV, more than 98.5% purity is required, and more than 99.0% purity is required according to United States Pharmacopeia XXV. In our previous study, it was clarified that famotidine, which is stable against light, was easily degraded and discolored with the addition of TiO_2.[5] Therefore, a preformulation study is essential to thoroughly clarify the effect of TiO_2 addition on drug decomposition, in order to maintain the high quality of pharmaceutical products containing this excipient.

The photocatalytic activity of TiO_2 has not been defined directly and is estimated by either the degree of discoloration or degradation of photolabile compounds. In this study, nisoldipine (isobutylmethyl-1,4-dihydro-2,6-dimethyl-4-(2′-nitrophenyl)-pyridine-3,5-dicarboxylate, NS), known as an excellent calcium channel blocker, was used as a target compound and the effect of TiO_2 addition on the photodegradation of this drug was examined with regard to the photocatalytic activity of TiO_2. The relationship between the physiochemical properties of TiO_2 and the degree of photocatalytic activity of TiO_2 was also investigated.

Experimental

Materials Ten types of commercially available TiO_2 were used. Six of these were of the anatase form and the remainder was the rutile form. Anatase forms were obtained from Teika Co., Ltd. (A-1, A-5, A-6), Nacalai Tesque Inc. (A-2), Toho Titanium Co., Ltd. (A-3) and Freund Corporation (A-4). Rutile forms were obtained from Teika Co., Ltd. (R-1, R-4), Showa Chemical Co., Ltd. (R-2) and Toho Titanium Co., Ltd. (R-3). In order to strictly examine the effect of TiO_2 on photodegradation of NS, these samples were not surface coated with any material. NS was obtained from Permachem Asia, Ltd. All other chemicals and reagents were analytical grade.

Photodegradation Test The samples used for the photodegradation test were prepared as follows. NS was dissolved in methanol (1 mg/ml) and 50 μl of the solution was added onto 10 mg of each sample of TiO_2 powder. After thorough dispersion, the suspension was dried under vacuum.

Each sample was irradiated with a D65 lamp (illuminance: 3500 lx) at 25 °C in a light-irradiation tester (LIGHTTRON LT-120, Nagano Science, Japan). After the designated irradiation times, the amount of NS remaining in the sample was determined by HPLC. The average of three determinations was plotted as % NS remaining.

High-Performance Liquid Chromatography (HPLC) Analysis NS was analyzed using an HPLC system consisting of a solvent delivery system and an UV detector (LC-10Avp system, Shimadzu, Japan) at a detection wavelength of 235 nm, or a photodiode array detector (Model 996, Waters) at wavelengths in the range of 220—360 nm. The prepacked column (Mightysil RP-18, 5 μm, 4.6×150 mm, Merck) was operated at 35 °C with a flow rate of 1.7 ml/min. The mobile phase consisted of methanol : water (63 : 37 volume ratio). After irradiation, each sample was dissolved in the internal standard solution (methanolic solution of diphenyl) and an aliquot of 50 μl was injected into the chromatograph.

The amount of photodegradation products of NS, nitroso-pyridine derivative (isobutylmethyl-2,6-dimethyl-4-(2′-nitrosophenyl)-pyridine-3,5-dicarboxylate, NTS) and nitro-pyridine derivative (isobutylmethyl-2,6-dimethyl-4-(2′-nitrophenyl)-pyridine-3,5-dicarboxylate, NTR), was calculated from the ratio of specific extinction reported in previous literature.[6]

Characterization of TiO_2 Particles Specific surface areas of TiO_2 powders were determined using nitrogen gas adsorption apparatus (Flowsorb II model 2300, Shimadzu, Japan) at liquid nitrogen temperature.

FT-IR spectra were obtained by a powder-diffuse reflectance method on a Fourier Transform-infrared spectrophotometer (Spectrum One, PerkinElmer Japan) with analysis of the TiO_2 powder dispersed in KBr powder (sample concentration 5 w/w%).

Water loss on drying of TiO_2 was measured by a thermogravimetric method (Thermo Plus TG8120, Rigaku Denki, Japan), using approximately 7 mg samples in aluminum pans at a constant scanning speed of 10 °C/min between 35 and 100 °C, under a nitrogen gas flow (100 ml/min).

Relative crystallinity was determined using powder X-ray diffraction[7] (RINT Ultima, Rigaku Denki, Japan) with nickel-filtered Cu$K\alpha$ radiation

* To whom correspondence should be addressed. e-mail: k-kakinoki@taiho.co.jp

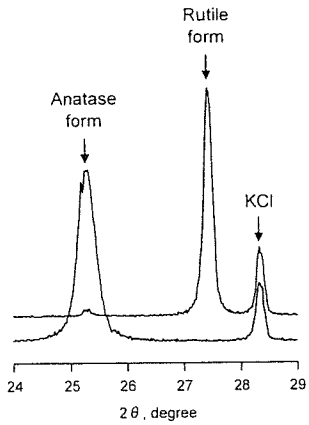

Fig. 1. Powder X-Ray Diffraction Patterns for the Anatase (A-5) and Rutile Forms (R-4) of TiO_2 and KCl

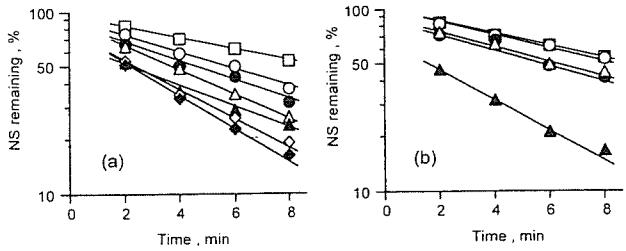

Fig. 2. The Effect of Various Types of TiO_2 Powders on the Photodegradation of NS under Irradiation with a D65 Lamp

(a) Anatase form; (○) A-1, (●) A-2, (△) A-3, (▲) A-4, (◇) A-5, (◆) A-6, (□) NS only, and (b) rutile form; (○) R-1, (●) R-2, (△) R-3, (▲) R-4, (□) NS only.

(30 kV, 30 mA) in the 2θ range from 20 to 80°. The scan speed was 4°/min and the scan time constant was 1 s. Relative crystallinity was calculated by the area ratio of peaks attributable to either anatase (2θ=25.4°) or rutile (2θ=27.4°) to that of KCl powder (2θ=28.4°), which was used as an internal standard (Fig. 1).

Results

Photocatalytic Activity of TiO_2 Figure 2 shows the effect of the various types of TiO_2 powders on the time course of photodegradation of NS. NS without TiO_2 was rapidly degraded and the percentage of NS remaining decreased to 53% after 8 min irradiation. With addition of TiO_2 to NS, the photodegradation process was significantly accelerated, but the degree of photodegradation acceleration was quite different among the different types of TiO_2. In Fig. 2, R-1 did not show any remarkable effect on the photodegradation of NS, whereas A-6 and R-4 exhibited a remarkable acceleration effect to photodegradation, and the percentage of NS remaining decreased to only 16% after 8 min irradiation. These photodegradation processes apparently followed a first order reaction. Thus, Table 1 shows the apparent photodegradation rate constants of NS for the various types of TiO_2. It is evident that the photocatalytic activity of TiO_2 was quite different among the various types of TiO_2, even if the crystalline phase was the same. In particular, R-4 showed a higher photocatalytic activity than any of the anatase forms, except for A-6. However, the other three types of rutile form displayed lower photocatalytic activity than those of anatase forms.

Figure 3 shows the HPLC chromatograms of samples obtained after 8 min irradiation. There were two peaks excepting NS (I) and internal standard (IS) at the same relative retention time in the three chromatograms, (A), (B), (C). The

Table 1. Apparent Photodegradation Rate Constants for Various Types of TiO_2

k, min^{-1}			
Anatase form		Rutile form	
A-1	0.117	R-1	0.073
A-2	0.136	R-2	0.108
A-3	0.203	R-3	0.103
A-4	0.162	R-4	0.220
A-5	0.172		
A-6	0.221		

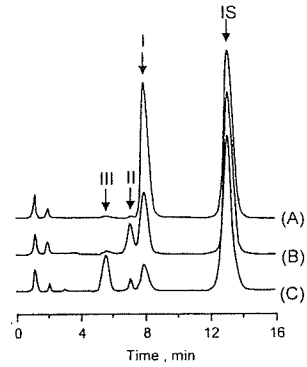

Fig. 3. HPLC Chromatograms for (A) NS, (B) NS after 8 min Irradiation with a D65 Lamp and (C) NS with TiO_2 (A-6) after 8 min Irradiation with a D65 Lamp

Each peak was assigned as (I) NS, (II) NTS and (III) NTR, respectively.

Table 2. Characteristics of NS and Photodegradation Products

Peak No.	Compound	Relative retention time to IS	Maximum absorption wavelengths, nm
I	Nisoldipine (NS)	0.60	239, 339
II	Nitroso-pyridine derivative (NTS)	0.54	281, 315
III	Nitro-pyridine derivative (NTR)	0.42	272

IS: internal standard.

maximum absorption wavelengths for each peak are shown in Table 2. These maximum absorption wavelengths were compared to the results reported in previous literature.[6] So, peaks II and III were identified as those of NTS and NTR, respectively. Photodegradation of NS without TiO_2 resulted in mainly NTS as a direct photooxidation product. On the contrary, NS concurrently formed two kinds of photodegradation products, NTS and NTR, with the addition of TiO_2. In particular, after the addition of A-6 to NS, the degree of NTR formation significantly increased compared with that of NTS formation (Fig. 4). This fact suggests that NTR is a degradation product derived from photocatalytic oxidation. The formation ratio of NTR to NTS for each sample after 8 min irradiation is summarized in Table 3. Figure 5 shows the relationship between the formation ratio of NTR to NTS and the apparent degradation rate constant of NS. Good correlation was established between the product formation ratio and degradation rate constant for all of these crystal forms (r=0.971, p<0.05 for anatase, n=6 and r=0.977, p<0.05 for rutile form, n=4). Therefore, the formation ratio of NTR to NTS is defined hereafter as the index of photocatalytic activity of TiO_2.

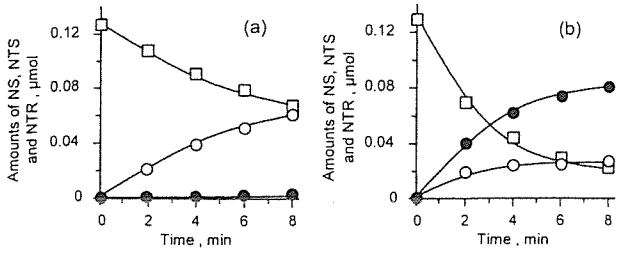

Fig. 4. Effect of TiO_2 (A-6) on the Photodegradation Time-Courses of NS and Formation of Photodegradation Product

(a) NS only; (b) NS with TiO_2. Key: (□) NS; (○) NTS; (●) NTR.

Table 3. Formation Ratio of NTR to NTS for Various Types of TiO_2 after 8 min Irradiation

Formation ratio of NTR to NTS			
Anatase form		Rutile form	
A-1	0.172	R-1	0.255
A-2	0.306	R-2	0.638
A-3	2.47	R-3	1.08
A-4	1.11	R-4	2.59
A-5	0.961		
A-6	2.95		

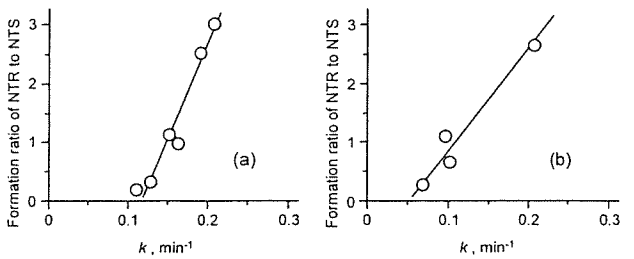

Fig. 5. Relationship between the Apparent Photodegradation Rate Constant, k and the Formation Ratio of NTR to NTS

(a) Anatase form; (b) rutile form.

Table 4. Specific Surface Area of Various Types of TiO_2

Specific surface area, m^2/g			
Anatase form		Rutile form	
A-1	8.19	R-1	5.38
A-2	14.9	R-2	13.8
A-3	22.7	R-3	17.6
A-4	23.6	R-4	78.2
A-5	44.2		
A-6	117.6		

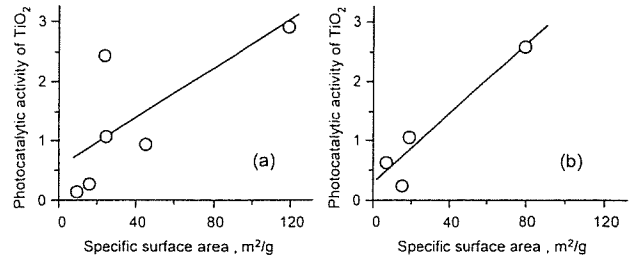

Fig. 6. Relationship between Specific Surface Area and Photocatalytic Activity of TiO_2

(a) Anatase form; (b) rutile form.

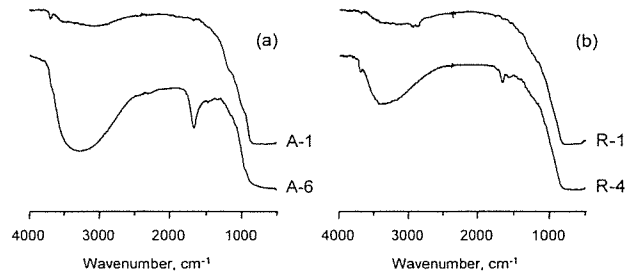

Fig. 7. Absorption Peaks in the FT-IR Spectra of TiO_2 Powders

(a) Anatase form; (b) rutile form.

Characterization for Photocatalytic Activity of TiO_2

The specific surface area of TiO_2 has been generally considered as a controlling factor of the photocatalytic activity: the light exposure area and number of reaction sites on the surface of TiO_2 powder would necessarily increase with an increase in specific surface area. Table 4 shows the specific surface area of the various types of TiO_2 investigated. For the anatase form, the smallest specific surface area was 8.19 m^2/g (A-1) and the largest was 117.6 m^2/g (A-6). For the rutile form, the smallest specific surface area was 5.38 m^2/g (R-1) and the largest was 78.2 m^2/g (R-4), indicating that the specific surface area was quite different even though the crystal phase was the same. Figure 6 shows the relationship between the specific surface area of various types of TiO_2 and their photocatalytic activity. For the both crystal forms, good correlations were observed between them. Particularly, a correlation for the rutile form (r=0.951, n=4) was better than that for the anatase form (r=0.738, n=6).

The amount of binding water associated with TiO_2 has also been considered as a contributing factor to photocatalytic activity, because our previous study[5] confirmed that relative humidity remarkably affects photocatalytic activity of TiO_2, and that water molecules in the atmosphere have an important role in the photocatalytic activity of TiO_2. Figure 7 shows the FT-IR spectra of TiO_2. From these results, the broad absorption peak in the wavenumber range from 2500 to 3900 cm^{-1} and the peak at 1600 cm^{-1} were appreciably different among the samples of TiO_2. These absorption peaks are closely related with stretching vibrations of the hydroxyl functional group.[11] Thus, to clarify the effect of water adsorption, the loss of water on drying of TiO_2 was measured. Table 5 shows water loss on drying for various types of TiO_2 powder, and Fig. 8 shows the relationship between the water loss and photocatalytic activity. Contrary to the results in Fig. 6, a relatively strong correlation was observed for the anatase form (r=0.712, n=6), whereas a very poor correlation was seen for the rutile form (r=0.498, n=4).

Finally, the relationship between the photocatalytic activity and crystallinity of TiO_2 was investigated. The difference in the crystal structure has been generally recognized as a factor closely related to the difference in photocatalytic activity between the anatase and rutile forms. The relative crystallinity of the various types of TiO_2 is summarized in Table 6, and the relationship between the relative crystallinity and photocat-

Table 5. Water Loss on Drying for Various Types of TiO_2

Water loss on drying, %			
Anatase form		Rutile form	
A-1	0.12	R-1	0.10
A-2	0.15	R-2	0.07
A-3	0.31	R-3	0.11
A-4	0.22	R-4	0.11
A-5	0.71		
A-6	6.48		

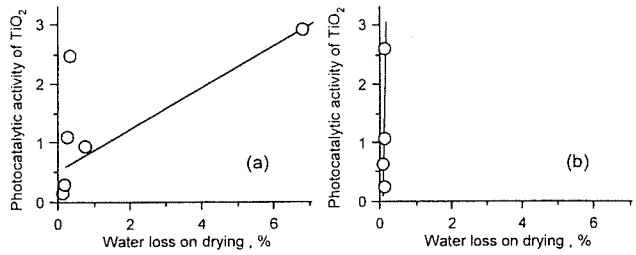

Fig. 8. Relationship between the Water Loss on Drying and Photocatalytic Activity of TiO_2

(a) Anatase form; (b) rutile form.

Table 6. Relative Crystallinity of Various Types of TiO_2

Relative crystallinity			
Anatase form		Rutile form	
A-1	5.97	R-1	4.65
A-2	6.79	R-2	4.72
A-3	3.37	R-3	3.70
A-4	5.56	R-4	3.34
A-5	2.99		
A-6	1.83		

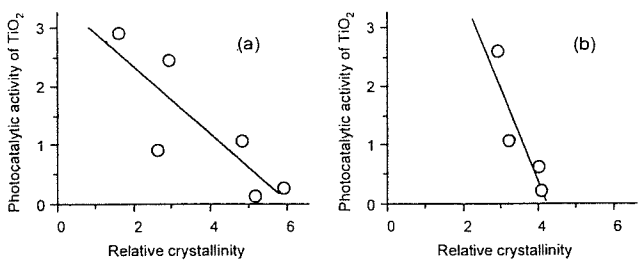

Fig. 9. Relationship between Relative Crystallinity and Photocatalytic Activity of TiO_2

(a) Anatase form; (b) rutile form.

alytic activity is shown in Fig. 9. A good correlation was established between these for all of the crystal forms (r=0.837 for anatase, n=6 and r=0.898 for rutile form, n=4).

Discussion

The photodegradation of NS by light irradiation was more or less enhanced by addition of TiO_2, and the difference in the degree of photodegradation was caused by the difference of photocatalytic activity. Particularly, for the rutile form, R-1 had little effect on the degradation of NS. On the other hand, R-4 showed a high photodegradation effect as did A-6, which exhibited higher photocatalytic activity than that of

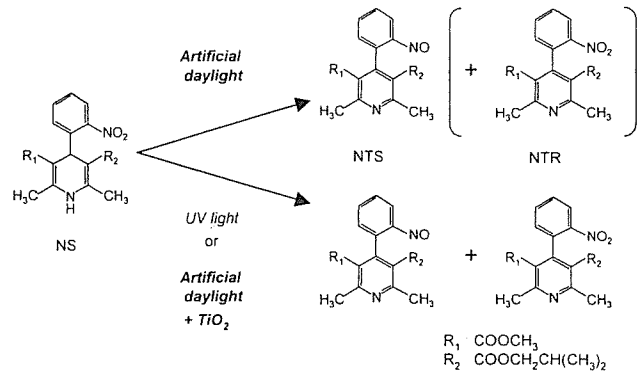

Fig. 10. Possible Photodegradation Processes of NS

any other anatase form measured. These facts suggest that the photocatalytic activity depends not only on the crystal form, but also on the other physicochemical properties of each type of TiO_2.

In the photodegradation processes, two kinds of photodegradation products, NTS and NTR, have been detected. It has been reported that NTS was a direct photooxidation product of NS under irradiation with artificial daylight or white fluorescent light,[8,9] whereas NTR is predominantly formed under UV light irradiation.[9,10] Therefore, in the presence of TiO_2, NTR would be produced even if the light source has low irradiation energy (Fig. 10). In addition, as the formation ratio of NTR to NTS becomes larger with increasing photocatalytic activity, it can be said that NTR is a photocatalytic degradation product with TiO_2 present and after irradiation.

According to the results described above, it is clear that the photocatalytic activity of TiO_2 is dependent not only on the crystal form, but also on the micromeritic properties of TiO_2 powders. Therefore, the relationship between the photocatalytic activity of TiO_2 and the physiochemical properties of TiO_2 was investigated.

For anatase form, photocatalytic activity was correlated with both specific surface area and water loss on drying. Therefore, for the anatase form, changes in specific surface area and water loss on drying affect the photocatalytic activity of TiO_2. On the other hand, photocatalytic activity of the rutile form was quite well correlated with specific surface area, but not correlated with water loss from drying. The rutile form has little water adsorption, because the values of water loss on drying were very small. Therefore, for the rutile form, a change in the specific surface area dramatically affects the photocatalytic activity of TiO_2.

Additionally, it was clear that for both crystal forms an increase of relative crystallinity of TiO_2 led to a decrease of photocatalytic activity; the slope of the regression line for the rutile form was steeper than that for the anatase form (Fig. 9). This fact suggests that the relative crystallinity of the rutile form is more sensitive for photocatalytic activity.

According to these facts, it might be possible to predict the photocatalytic activity of TiO_2, particularly for the rutile form, by measuring the specific surface area of TiO_2. Previously, we discussed that the photocatalytic activity of TiO_2 can comprise the high quality and chemical integrity of pharmaceutical products. However, TiO_2 is an essential excipient, because of its whiteness and light-proofing ability. Therefore

the information on the relationship between photocatalytic activity and physicochemical properties of TiO_2 will be useful to make a rational selection of the appropriate type and grade of commercial TiO_2 for this use.

References

1) Fujishima A., Rao T. N., Tryk D. A., *J. Photochem. Photobiol. C*, **1**, 1—21 (2000).
2) Sabin F., Türk T., Vogler A., *J. Photochem. Photobiol. A*, **63**, 99—106 (1992).
3) Khalyavka T. A., Shimanovskaya V. V., Strelko V. V., Kapinus E. I., *Theor. Exp. Chem.*, **37**, 58—62 (2001).
4) Kang M., Lee S., Chung C., Cho S. M., Han G. Y., Kim B., Yoon K. J., *J. Photochem. Photobiol. A*, **144**, 185—191 (2001).
5) Kakinoki K., Yamane K., Teraoka R., Otsuka M., Matsuda Y., *J. Pharm. Sci.*, **93**, 582—589 (2004).
6) Vetuschi C., Ragno G., Veronico M., Risoli A., Ginnandrea A., *Anal. Lett.*, **35**, 1327—1339 (2002).
7) Ito S., Inoue S., Kawada H., Hara M., Iwasaki M., Tada H., *J. Colloid Interface Sci.*, **216**, 59—64 (1999).
8) Takahashi K., Noda H., Noda A., *Kyushu Yakugakkai Kaiho*, **47**, 37—43 (1993).
9) Marinkovic V. D., Agbaba D., Karljikovic-Rajic K., Vladimirov S., Nedeljkovic J. M., *J. Pharm. Biomed. Anal.*, **32**, 929—935 (2003).
10) Michelitsch A., Reiner J., Schubert-Zsilavecz M., Likussar W., *Pharmazie*, **50**, 548—549 (1995).
11) Kiyono M., "Sankatitan," Gihodo-shuppan, Japan, 1991, pp. 53—58.

Effect of Titanium Dioxide on Photostability of Solid-State Mequitazine

Koichi KAKINOKI,*[,a] Kenji YAMANE,[a] Manami YAMAMOTO,[b] Reiko TERAOKA,[b] Isao SUGIMOTO,[b] and Yoshihisa MATSUDA[b]

[a] *Formulation & Industrial Technology Lab., Taiho Pharmaceutical Co., Ltd.; Tokushima 771–0194, Japan: and* [b] *Department of Pharmaceutical Technology, Kobe Pharmaceutical University; Higashi-nada-ku, Kobe 658–8558, Japan.*
Received February 10, 2005; accepted June 1, 2005; published online June 3, 2005

TiO_2 has been widely used in pharmaceutical products, and it also has been used as a photocatalyst. In this study, the influence of photocatalytic activity on the stability of solid-state mequitazine, an H_1-blocker, was investigated. The photo-degradation of mequitazine with TiO_2 occurred under irradiation with both light sources. The degree of degradation of mequitazine with anatase was higher than that of rutile. The degradation was significantly enhanced with increasing relative humidity. The relationship between the apparent degradation rate constant and water vapor pressure could be clearly described by a simple power law. The major photo-degradation products of mequitazine, resulting from photocatalytic activity of TiO_2, were mequitazine-*S*-oxide and mequitazine-sulphone. A remarkable degradation of mequitadine occurred with addition of TiO_2, and its photocatalytic activity was controlled by water vapor pressure. The photo-degradation of mequitazine with TiO_2 is a different process from mequitazine without TiO_2, because mequitazine-*S*-oxide and mequitazine-sulphone are not formed with normal photo-degradation of mequitazine.

Key words preformulation; solid state stability; photostability; titanium dioxide; photocatalytic activity

Titanium dioxide (TiO_2) is known as a useful inorganic pigment and is widely used as a coating material for solid pharmaceutical preparations. Recently, many studies have been performed, from a material science perspective, to modify the function of TiO_2 as a strong photocatalyst. In some studies the photocatalytic activity of TiO_2 has been linked to oxidation-reduction reactions.[1—6]

With regard to pigment use, TiO_2 is usually surface-treated to prevent photocatalytic activity. On the other hand, for pharmaceutical use, TiO_2 is not surface-treated, and even if the surface is treated, the amount of surface coating substance would be very small, because of its strictly regulated purity. Thus, TiO_2 for pharmaceutical use may exhibit considerable photocatalytic activity. Therefore, when TiO_2 is used in pharmaceutical preparations, some drugs may often be easily decomposed by light irradiation. However, on pharmaceutical research field, almost studies were reported for the effect of light resistance of TiO_2 or the reaction related to TiO_2 in the solution system.[7—11] We focused the solid-state reaction between TiO_2 and drug substance. In our previous work, it was revealed that famotidine, known as an H_2-blocker, with TiO_2 as an additive, was easily discolored by only light, and the photocatalytic activity of TiO_2 was controlled by relative humidity.[12] Therefore, the purpose of this preformulation study is to clarify the relationship between the addition of TiO_2 and drug decomposition, so that from a thorough investigation, consistently high quality in pharmaceutical products may be assured.

Mequitazine, known as a histamine H_1-receptor antagonist, is slightly discolored under irradiation with light. On the basis of this fact, mequitazine may be unstable under light irradiation, and therefore it may be presumed that the photostability of mequitazine will be influenced by the photocatalytic activity of TiO_2. In this study, mequitazine was employed as a model drug for fundamental study and the effect of photocatalytic activity of TiO_2 on the solid-state photostability of mequitazine under various relative humidity conditions was investigated. The photodegradation products of irradiated mequitazine containing TiO_2 were also investigated.

Experimental

Materials Two commercially available crystal structures of TiO_2, anatase and rutile, were used. In order to examine the effect of TiO_2 on photodegradation of mequitazine, the surface of these TiO_2 powders was not coated with any material. The anatase and rutile forms of TiO_2 were supplied by Toho Titanium Co., Ltd. and Showa Chemical Co., Ltd, respectively. Mequitazine was obtained from Sumika Fine Chemicals Co., Ltd. Mequitazine-*N*-oxide and mequitazine-*S*-oxide were obtained from Azwell Inc. All other chemicals and reagents were analytical grade.

Discoloration Test The samples used for the discoloration test were prepared as follows: Mequitazine and TiO_2 were physically mixed in a bowl at a mass ratio of 1 : 1. A 200 mg sample of mixture was compressed into a 10 mm diameter pellet under a compression force of 10 kN, using an accurate compression/tension testing machine (Autograph model IS-5000, Shimadzu).

Samples were placed in a light-irradiation tester (LIGHTTRON LT-120, Nagano Science) at 25 °C and irradiated with a D65 lamp (illuminance: 3500 lx). Discoloration of the pellet surface, after irradiation, was measured using a chromameter (Model 300A, Nippon Denshoku) after the designated time points in the Lab color system.

Degradation Test The samples for the degradation test were prepared as follows: Mequitazine was dissolved in methanol (1 mg/ml) and 50 μl of the solution was added to 10 mg of TiO_2 powder. After thorough dispersion, this suspension was dried under vacuum. A solution of benzophenone in isooctane–methanol (1 : 1 v/v) was prepared as an internal standard for high-performance liquid chromatography (HPLC) analysis.

Each sample was placed in a desiccator at 0, 22, 75 and 97% RH at 25 °C and irradiated with a near-UV lamp (irradiation energy: 1.0 mW/cm^2) or a D65 lamp (illuminance: 3500 lx) in the light-irradiation tester (LIGHTTRON LT-120, Nagano Science). The amount of mequitazine remaining in the sample, with respect to time, was measured by HPLC. A relative humidity of 0% RH was maintained using diphosphorus pentaoxide, and others were adjusted using saturated aqueous solutions of several inorganic salts; 22% RH: potassium acetate, 75% RH: sodium chloride, and 90% RH: potassium sulfate.

HPLC Analysis Mequitazine was analyzed using an HPLC system consisting of a solvent delivery system (Model 510, Waters) and a UV detector (Model 484, Waters) at a detection wavelength of 254 nm, or a photodiode array detector (Model 996, Waters) at wavelengths of 250—360 nm. The prepacked column (Zorbax Rx-SiL, 5 μm, 4.6×250 mm, Agilent Technologies) was operated at room temperature with a flow rate of 1.5 ml/min. The mobile phase consisted of isooctane : ethanol : acetonitrile : isopropylamine : water (120 : 100 : 15 : 7 : 2 volume ratio). After irradiation, each sample was dissolved in the internal standard solution and after filtrated by

* To whom correspondence should be addressed. e-mail: k-kakinoki@taiho.co.jp

0.45 μm membrane filter, a 20 μl aliquot was injected into the chromatograph.

HPLC/APCI-MS Analysis Degradation products of mequitazine were completely identified by a high-performance liquid chromatography/atmospheric pressure chemical ionization-mass spectrometry (HPLC/APCI-MS) system. The HPLC system consisted of a solvent delivery system and a UV detector (LC-10Avp system, Shimadzu). The prepacked column (Lichrospher CN, 5 μm, 4×125 mm, Cica-Merk) was operated at room temperature with a flow rate of 1.8 ml/min. The mobile phase consisted of acetonitrile : methanol : isopropanol : water : 1 M ammonium acetate solution (85 : 5 : 5 : 6.65 : 0.35 volume ratio). The sample preparation was the same as that described previously for the HPLC analysis.

Mass spectrometric detection was achieved by means of an Applied Biosystems API 3000 apparatus using an APCI interface. MS measurements were acquired in positive ion, full scan modes from 100 to 400, using a fragmentation voltage of 80 V to determine the molecular weights of the degradation products.

Results

Figure 1 shows the effect of TiO_2 on the time course of surface discoloration for the mequitazine pellet at 25 °C. Mequitazine with a TiO_2 additive, for both crystal structures, was significantly discolored; whereas, without TiO_2, only slight discoloration was observed, even after a long period of irradiation (25 h). Discoloration of mequitazine with anatase additive was significantly greater than that with rutile. Figure 2 shows the effect of TiO_2 on the degradation of mequitazine with time at 25 °C and 75% RH. Under irradiation with both the near-UV and D65 lamps, mequitazine with anatase showed a remarkable degradation, but was only slightly degraded for rutile. Mequitazine without TiO_2 was hardly degraded, even after a long period of irradiation. The degradation rate of mequitazine was much higher under the near-UV lamp, than under the D65 lamp. This degradation process apparently followed a first order reaction. Figure 3 shows the degradation of mequitazine with TiO_2 with respect to time, at various relative humidity, with irradiation using near-UV light. The degree of degradation increased with increasing relative humidity for both TiO_2 crystal forms, and particularly for anatase, the increment of degradation was greater. The phenomenon for irradiation observed under the near-UV lamp was also observed under the D65 lamp (Fig. 4). Figure 5 shows the semi-logarithmic plots of the relationship between the apparent degradation rate constant, calculated from the slopes of regression lines in Figs. 3 and 4, and the water vapor pressure, converted from relative humidity, under each

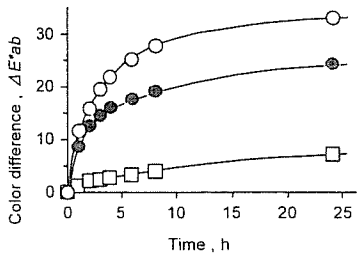

Fig. 1. The Effect of Photocatalytic Activity of TiO_2 on the Discoloration of Mequitazine at 25 °C under Irradiation by a D65 Lamp

(○) With anatase, (●) with rutile, and (□) without TiO_2.

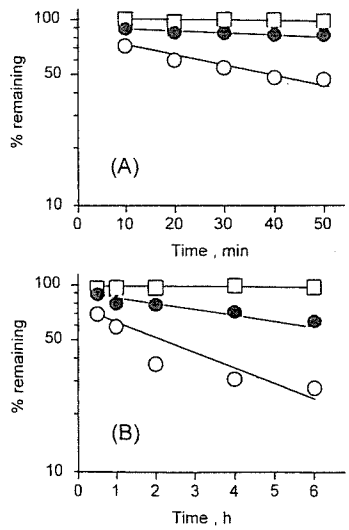

Fig. 2. The Effect of Photocatalytic Activity of TiO_2 on the Degradation of Mequitazine at 25 °C and 75% RH and under Irradiation by (A) a Near-UV Lamp and (B) a D65 Lamp

(○) With anatase, (●) with rutile, and (□) without TiO_2.

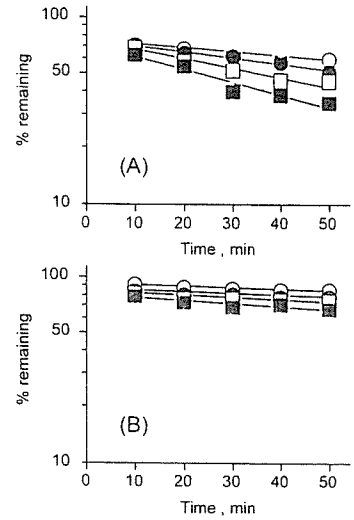

Fig. 3. The Effect of Relative Humidity on the Degradation of Mequitazine at 25 °C under Irradiation by a Near-UV Lamp: (A) with Anatase; and (B) with Rutile

(○) 0% RH, (●) 22% RH, (□) 75% RH, (■) 97% RH.

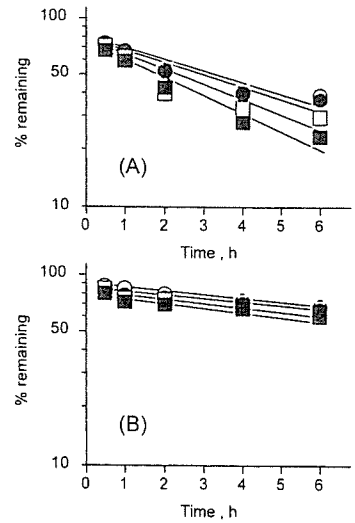

Fig. 4. The Effect of Relative Humidity on the Degradation of Mequitazine at 25 °C under Irradiation by a D65 Lamp: (A) with Anatase; and (B) with Rutile

(○) 0% RH, (●) 22% RH, (□) 75% RH, (■) 97% RH.

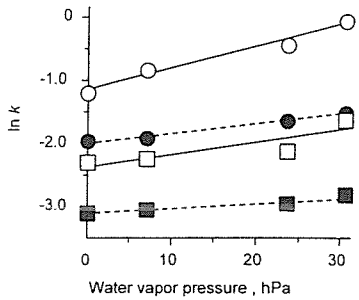

Fig. 5. The Effect of Water Vapor Pressure on the Degradation Rate Constant

(○) With anatase under irradiation by a near-UV lamp and (●) with anatase under a D65 lamp; (□) with rutile under irradiation by a near-UV lamp and (■) with rutile under a D65 lamp.

Table 1. r-Values under the Various Irradiation Conditions

Light source	r ($\times 10^3$)	
	Anatase system	Rutile system
Near-UV lamp	33.5	18.0
D65 lamp	14.0	8.2

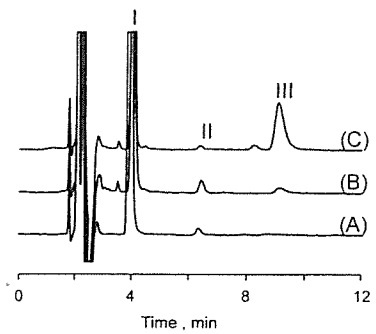

Fig. 6. HPLC Chromatograms of the Sample after 50 min Irradiation by a Near-UV Lamp at 25 °C and 97% RH; (A) Mequitazine, (B) Mequitazine with Rutile, (C) Mequitazine with Anatase

Each peak is assigned as (I) mequitazine, (II) mequitazine-*N*-oxide and (III) mequitazine-*S*-oxide.

light source. Good linear relationships were established between the logarithm of the apparent degradation rate constant and the water vapor pressure, for either of the TiO_2 crystal forms. The apparent degradation rate constant for anatase was larger than that for rutile, at all water vapor pressures under any of the light sources. This fact clearly indicates that anatase exhibits higher photocatalytic activity than rutile. These results imply a relationship between the apparent degradation rate constant and water vapor pressure as shown in Eq. 1

$$\ln k = \ln k_0 + r \cdot P \quad (1)$$

where P is the water vapor pressure, r is a coefficient relating to water vapor pressure dependency of the apparent degradation rate constant, and k_0 is the apparent degradation rate constant calculated for 0% RH. The values of r, calculated from Eq. 1, are given in Table 1.

Figure 6 shows the HPLC chromatograms of samples after 6 h irradiation with the D65 lamp at 25 °C and 97% RH. Each of the peaks I, II and III were identified to be

Table 2. UV and HPLC Characteristics of Mequitazine and Related Compounds

Peak	Compound	Retention time (min)	Maximum UV absorbance (nm)
I	Mequitazine	4.03	308
II	Mequitazine-*N*-oxide	6.45	308
III	Mequitazine-*S*-oxide	9.12	278, 300, 346

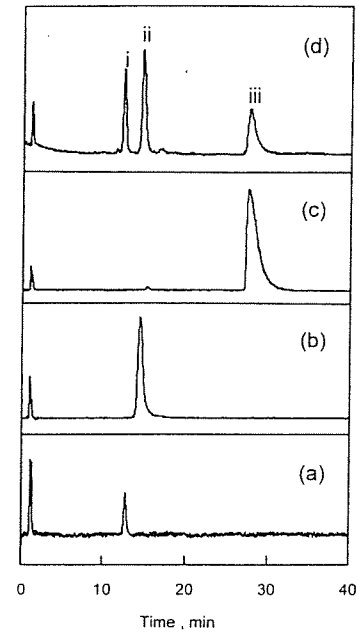

Fig. 7. HPLC Chromatograms for MS Analysis of the Standard with (a) Mequitazine, (b) Mequitazine-*N*-oxide, (c) Mequitazine-*S*-oxide and (d) Mequitazine with Anatase after 50 min Irradiation by a Near-UV Lamp at 25 °C and 97% RH

mequitazine, mequitazine-*N*-oxide and mequitazine-*S*-oxide, respectively, by their UV spectrum. The characteristics of each peak obtained from the HPLC chromatograms and UV spectra are shown in Table 2. Interestingly, degradation of mequitazine without TiO_2 produced only mequitazine-*N*-oxide as the degradation product; however, mequitazine with TiO_2 gave two kinds of degradation products; mequitazine-*N*-oxide and mequitazine-*S*-oxide.

The degree of mequitazine-*S*-oxide formation for mequitazine with anatase was particularly larger than that for rutile. HPLC/APCI-MS analysis was used as another approach to identify the photodegradation products. The condition for the HPLC-MS was not the same as that described for the HPLC analysis, because the degradation products could not be ionized under the former condition. Figure 7 shows the chromatograms of these photo degradation products. The *m/z* value of each peak was determined by MS analysis, as shown in Fig. 8. The retention time on the chromatogram and the *m/z* value of the peak (d)-i correspond to that of intact mequitazine, and peak (d)-iii corresponds to that of the standard sample of mequitazine-*S*-oxide. On the contrary, the retention time and the *m/z* value of peak (d)-ii did not correspond to that of the standard sample of mequitazine-*N*-oxide. From the results of previous reports,[13] (d)-ii was presumed to be mequitzine-sulphone, because the *m/z* value (355.4) of the (d)-ii peak coincided with that of mequitazine-sulphone.

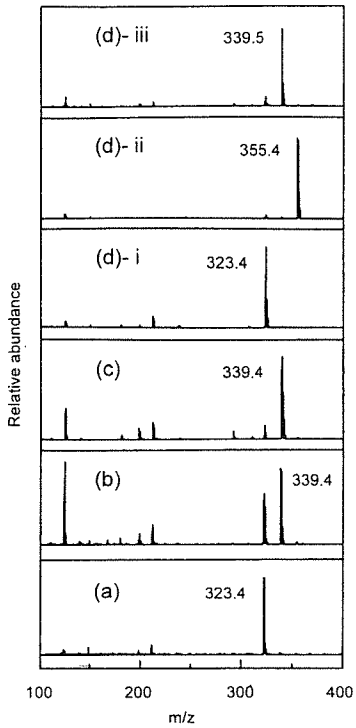

Fig. 8. Mass Spectroscopic Peaks Obtained from HPLC Chromatography *cf.* Fig. 7.

At this retention time, mequitazine-*N*-oxide could not be detected, due to the difficulty of ionizing mequitazine-*N*-oxide under these HPLC-MS analysis conditions. According to these results, it was confirmed that at least three kinds of photo-degradation products, mequitazine-*N*-oxide, mequitazine-*S*-oxide and mequitazine-sulphone were formed from mequitazine.

Discussion

Mequitazine, with the addition of TiO_2, was easily degraded by light irradiation. The degree of degradation for mequitazine with anatase was larger than that with rutile, under all experimental conditions. This fact can lead to the conclusion that the photocatalytic activity of anatase is higher than that of rutile. The photocatalytic activities of these TiO_2 phases have been measured by a direct electrochemical measuring method, four-probe method.[12] The degradation of mequitazine occurred under irradiation with not only a near-UV lamp, but also a D65 lamp. The rate of degradation of mequitazine with a near-UV lamp was faster than that with a D65 lamp for both crystal forms because the energy giving an excitation state of a near-UV lamp would be stronger than that of a D65 lamp. Since D65 lamps have been widely used as a standard light source for the light stability test, the quality of pharmaceutical preparations containing photo-labile drugs such as mequitazine with TiO_2, are easily-deteriorated by light irradiation. The degradation of mequitazine with TiO_2 was remarkably enhanced by an increase of relative humidity. The relationship between water vapor pressure and the apparent degradation rate constant could be described by a simple power low. Since the same tendency was observed in our previous study,[12] this fact suggests that the photocatalytic activity of the two TiO_2 phases is controlled by water vapor pressure. Furthermore, during the

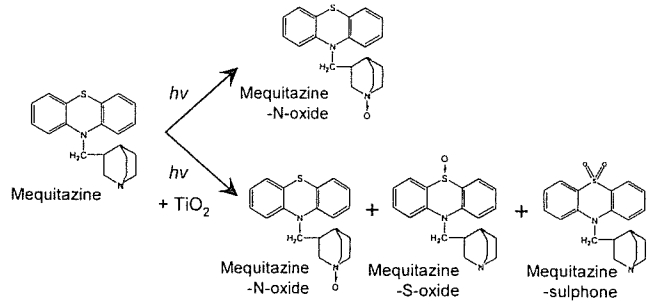

Fig. 9. Degradation Scheme of Mequitazine and Mequitazine with TiO_2 upon Exposure to Light

degradation process, the ratio of the *r*-value for anatase to that for rutile, under the near-UV lamp, was calculated to be 1.71. This value was similar to that under the D65 lamp, calculated as 1.86. This result also suggests that the dependency of the ratio of the *r*-value for anatase to that for rutile on water vapor pressure would be almost constant, even under a different type of light source.

Three kinds of photodegradation products of mequitazine were detected in this study; mequitazine-*N*-oxide, mequitazine-*S*-oxide and mequitazine-sulphone. It was confirmed that mequitazine-*N*-oxide was a direct photooxidation product of mequitazine, because it was obtained by light irradiation of pure mequitazine, without TiO_2.[14] On the other hand, mequitazine-*S*-oxide and mequitazine-sulphone were photocatalytic degradation products after irradiation of mequitazine with TiO_2 additive. According to these results, the following degradation mechanism may be possible: The degradation caused by photocatalytic activity of TiO_2 would predominantly oxidize the sulfur part of the mequitazine molecule, as shown in Fig. 9. Mequitazine-sulphone has been reported as a degradation product of mequitazine reacted with hydrogen peroxide.[13] Some studies have described that the radicals are generated due to photocatalytic activity of TiO_2.[1,15,16] In the series of radical reactions, the generation of hydrogen peroxide may be considered as follows:

$$TiO_2 + h\nu \rightarrow e^- + h^+$$

$$e^- + O_2 \rightarrow \cdot O_2^-$$

$$\cdot O_2^- + H^+ \leftrightarrow HO_2\cdot$$

$$2HO_2\cdot \rightarrow H_2O_2 + O_2$$

Moisture proofing is important to restrain the photocatalytic activity of TiO_2 in pharmaceutical preparations of photo-labile drugs, because moisture can play an important role in the degradation reaction.

Conclusion

Mequitazine was significantly degraded by photocatalytic activity of TiO_2 under light irradiation and this degradation was enhanced by increasing the relative humidity under various storage conditions. Because the relationship between the relative humidity and the apparent degradation rate constant was described with a simple power law, the photocatalytic activity of TiO_2 was confirmed to be controlled by moisture adsorption onto mequitazine crystals. The degradation products of mequitazine with TiO_2 were different from that formed from mequitazine without TiO_2. By the interaction between

TiO_2 and mequitazine, unexpected photo-degradation products could be identified. So using TiO_2 for pharmaceutical products, we must be care of unexpected photo-degradation products from ingredient.

References

1) Fujishima A., Rao T. N., Tryk D. A., *J. Photochem. Photobiol. C*, **1**, 1—21 (2000).
2) Sabin F., Türk T., Vogler A., *J. Photochem. Photobiol. A*, **63**, 99—106 (1992).
3) Davydov L., Reddy E. P., France P., Smirniotis P. G., *Appl. Catal. B*, **32**, 95—105 (2001).
4) Khalyavka T. A., Shimanovskaya V. V., Strelko V. V., Kapinus E. I., *Theor. Exp. Chem.*, **37**, 58—62 (2001).
5) Kang M., Lee S., Chung C., Cho S. M., Han G. Y., Kim B., Yoon K. J., *J. Photochem. Photobiol. A*, **144**, 185—191 (2001).
6) Heredia J. B. D., Torregrosa J., Dominguez J. R., Peres J. A., *J. Hazard. Mater.*, **B83**, 255—264 (2001).
7) Matsuda Y., Inoue H., Nakanishi R., *J. Pharm. Sci.*, **67**, 196—201 (1978).
8) Matsuda Y., Itooka T., Mitsuhashi Y., *Chem. Pharm. Bull.*, **28**, 2665—2671 (1980).
9) Teraoka R., Matsuda Y., Sugimoto I., *J. Pharm. Pharmacol.*, **41**, 293—297 (1988).
10) Franch M. I., Ayllon J. A., Peral J., Domenech X., *Catal. Today*, **76**, 221—233 (2002).
11) Doll T. E., Frimmel F. H., *Water Res.*, **38**, 955—964 (2004).
12) Kakinoki K., Yamane K., Teraoka R., Otsuka M., Matsuda Y., *J. Pharm. Sci.*, **93**, 582—589 (2004).
13) El-Ragehy N. A., Badawey A. M., Khateeb S. Z., *J. Pharm. Biomed. Anal.*, **29**, 121—137 (2002).
14) Asahi Kasei Pharma Co. Interviewform Zesulan' Tablets (2003).
15) Augugliaro V., Coluccia S., Loddo V., Marchese L., Martra G., Palmisano L., Schiavello M., *Appl. Catal. B*, **20**, 15—27 (1999).
16) Allen N. S., Katami H., *Polym. Degrad. Stab.*, **52**, 311—320 (1996).

Pharmaceutical Research, Vol. 23, No. 4, April 2006 (© 2006)
DOI: 10.1007/s11095-006-9644-7

Research Paper

Crystalline Form Information from Multiwell Plate Salt Screening by Use of Raman Microscopy

Takashi Kojima,[1,2,3] Satomi Onoue,[2] Noriaki Murase,[2] Fumie Katoh,[1] Takashi Mano,[2] and Yoshihisa Matsuda[1]

Received August 23, 2005; accepted December 2, 2005

Purpose. The purpose of this study was to establish a useful methodology, possibly providing information on the stoichiometry of pharmaceutical drug salts obtained from salt screening by using a multiwell plate and a Raman microscope.
Methods. Tamoxifen salt screening was conducted with monobasic and polybasic acids on 96-well quartz plates with a Raman microscope. Appearance and crystalline forms of salts prepared on 96-well plates were observed by polarizing light microscope and Raman microscope, respectively. Based on the results of the salt screening, tamoxifen citrate and fumarate salts were prepared on a large scale. The salts prepared were characterized by powder X-ray diffractometry (PXRD) and ion chromatography.
Results. The results of the multiwell salt screening indicated that tamoxifen has a tendency toward the formation of mono salt as opposed to hemi salt with polybasic acid, and that most of tamoxifen salts gave several potential polymorphic forms. PXRD patterns of scaled-up tamoxifen citrate and fumarate salts suggested that the same crystalline form was obtained from the binary mixture regardless of molar ratios of 2:1 or 1:1 (tamoxifen/acid). The crystalline forms obtained were tamoxifen monocitrate and monofumarate salts as measured by ion chromatography.
Conclusions. Salt screening on multiwell plates with a Raman microscope provided novel insight into the characteristics prediction of the stoichiometrical salts in addition to potential polymorph information. Based on the stoichiometrical information of salts, the amount of compound and time required for crystalline form selection of drug candidates would be significantly reduced.

KEY WORDS: crystalline form; polymorphism; Raman microscope; salt screening; tamoxifen.

INTRODUCTION

In the field of drug development, solid form selection of pharmaceutical compounds, such as crystalline and amorphous, is an essential process, because selected solids can dominate physicochemical properties affecting the efficacy, safety (1–3), stability (4), manufacturing process (5,6), and quality control (7). Especially, crystalline form selection has gotten a lot of attention recently. For example, inadequate crystalline form selections have resulted in the withdrawal of products from the market (8,9). Moreover, insufficient crystalline form screening has led to patent litigation (10). To avoid these problems, many articles have discussed a crystalline form selection strategy comprised of salt screening, polymorph screening, and crystalline form characterization (4,11–18).

Although significant progress in the computational prediction of polymorphs has been made in the past decade (19), the packing structure of crystals in salt and pseudopolymorphic systems, as yet, cannot be predicted, and experimental salt and polymorph screening is still relied on. To reveal or validate polymorphs, numerous studies dealing with high-throughput salt and polymorph screening have been conducted because polymorph or pseudopolymorph would be given under the wide range of solvent and crystallization conditions (20–29). High-throughput salt and polymorph screening is commonly performed using a multiwell plate, powder X-ray diffractometry (PXRD), and a Raman microscope. Raman microscopy is especially useful for salt screening because the technique has made it possible to obtain not only physical information but also chemical information (30,31). The flood of data provided by high-throughput equipment can be automatically analyzed by computer using classification software (32–34). These techniques for crystalline form identification from physical information have been currently applied to high-throughput salt and polymorph screening. However, chemical information specific to high-throughput salt and polymorph screening

[1] Department of Pharmaceutical Technology, Kobe Pharmaceutical University, Higashi-Nada, Kobe 658-8558, Japan.
[2] Science and Technology, Pfizer Global Research and Development, Nagoya Laboratories, Pfizer Japan Inc., 5-2 Taketoyo, Aichi 470-2393, Japan.
[3] To whom correspondence should be addressed. (e-mail: takashi.kojima@pfizer.com)

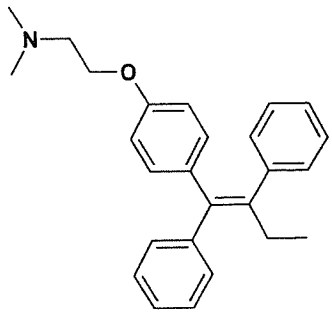

Fig. 1. Chemical structure of tamoxifen.

with a Raman microscope has not been fully elucidated up to now.

This paper focuses on salt screening through the use of multiwell plates and Raman microscopy using tamoxifen (Fig. 1) as a model drug. Tamoxifen is clinically used as an antiestrogenic agent for the treatment of breast cancer (35) and marketed as a monocitrate salt.

In this study, we performed effective salt screening on tamoxifen by using Raman microscopy to evaluate chemical information. Some of the salts obtained were also separately prepared on a large scale, characterized, and compared with the results of salt screening on multiwell plates using a Raman microscope. In addition, information obtained by using this combination technique was discussed.

MATERIALS AND METHODS

Materials

Tamoxifen free base was obtained from Aldrich Chemical Company (Milwaukee, WI, USA). Methanesulfonic acid was obtained from Nacalai Tesque (Kyoto, Japan), and other organic acids were obtained from Wako Pure Chemical Industries (Osaka, Japan). All solvents were purchased from Wako Pure Chemical Industries.

Salt Screening on 96-Well Plate

Tamoxifen salt formation on a 96-well plate was conducted using a combination of 12 kinds of crystallization solvents and six different acids according to the method reported (25). Each methanol solution of tamoxifen and acids, which were methanesulfonic acid and benzenesulfonic acid as monobasic acids, and L-tartaric acid, fumaric acid, citric acid, and succinic acid as polybasic acids, was prepared in the same concentration of 20 mM prior to use. Tamoxifen solution (50 μl) was placed in all wells of the 96-well quartz plate (Hellma, Müllheim, Germany). Each aqueous solution of monobasic acid (50 μl) was added into each row of the plate to give the binary mixture of tamoxifen and acid in a molar ratio of 1:1. Each aqueous solution of polybasic acid (25 or 50 μl) was added to give 2:1 or 1:1 binary mixtures of tamoxifen and acid in the same manner as monobasic acid solution. The plate was sealed with CAPMATS (Whatman, Brentford, UK) and was shaken with BioShaker M·BR-022 (TAITEC, Saitama, Japan) at room temperature for 4 h. Solvent was evaporated under reduced pressure at 40°C overnight. Each crystallization solvent, 200 μl of methanol, ethanol, isopropyl alcohol, acetonitrile, acetone, ethyl acetate, isopropyl ether, tetrahydrofuran, toluene, dichloromethane, cyclohexane, and 100 μl of water, was added to each column of the plate. The plate was sealed again and shaken at 40°C for 4 h and allowed to stand at room temperature overnight. All solvents in the plate were evaporated slowly in an atmosphere of nitrogen to attempt crystallization. Solids recrystallized on the 96-well plate were checked for crystallinity with a polarizing light microscope (PLM) and analyzed with Raman microscope (n = 2 in each well).

Salt Preparation

Tamoxifen fumarate and citrate salts were prepared on a 300-mg scale. Tamoxifen free base was dissolved in acetonitrile, and fumaric or citric acid was added to give 1:1 and 2:1 (tamoxifen/acid) mixtures. The suspension obtained was dried under reduced pressure. The resultant products were recrystallized by slowly cooling the saturated solution from the same 12 solvents as those for the salt screening on the 96-well plate, filtrated and dried in an atmosphere of nitrogen. Crystals obtained were subjected to PXRD and ion chromatographic analysis.

Raman Microscopy

Raman spectra were recorded on a LabRam HR-800/HTS-Multiwell (Jobin Yvon Horiba, Edison, NJ, USA) at room temperature, equipped with a backscattering light path system of a light-emitting diode laser (785 nm, 300 mW) as an excitation source and an air-cooled charge-coupled device detector. A 20-fold superlong working distance objective lens was used to collect the backscattered light. The spectra were acquired with 5.84 cm^{-1} spectral width and at least 30 s exposure. The laser power incident on the sample was 87mW. The spectrometer was calibrated with a silicon wafer.

Powder X-Ray Diffractometry

Powder X-ray diffraction patterns were collected using an RINT-TTR (Rigaku, Tokyo, Japan) with Cu Kα radiation generated at 300 mA and 50 kV. Samples were placed on an aluminum rotation plate and rotated at 60 rpm at room temperature. Data were collected from 3 to 35 (2θ) at a step size of 0.02° and scanning speed of 4°/min.

Ion Chromatography

Ion chromatography was performed using a Dionex (Sunnyvale, CA, USA) DX 500 apparatus equipped with a GP50 pump and an AS50 autosampler, connected to a CD25 conductivity meter with Peaknet software. Potassium hydroxide eluent was generated electrolytically using a Dionex EG40 eluent generator, and multistep gradient concentrations ranging from 10 to 60 mM allowed the complete separation of counterions in aqueous media in 15ômin at a constant flow rate of 1.0 ml/min. An ASRS Ultra II suppressor at 100 mA, with an external water feed, was used for anion chromatography.

Table I. Raman Spectra Classification of Tamoxifen Salts on 96-Well Plates

	Counter acids	TAM : CA	Solvents											
			MeOH	EtOH	IPA	MeCN	Acetone	EtOAc	IPE	THF	Toluene	DCM	cHex	Water
1	Methanesulfonic acid [a]	1 : 1	M1	M1	M1	M1	M1	M1	M1	M1	M2	M2	M1	–
2	Benzenesulfonic acid [b]	1 : 1	–	B2	B1	B2	–	B1	B1	–	B2	B2	B1	B2
3	L-Tartaric acid [c]	1 : 1	T1	T1	T1	T1	T1	T1	T3	T1	T1	T2	T1	T1
4	L-Tartaric acid [c]	2 : 1	T2	T1	T2 Free	T1	T2	T2	T2 Free	T1	T1	T1	T2	T2
5	Fumaric acid [d]	1 : 1	F2	F1	F1	F1	F1	F1 F2	F2	F2	F2 CA	F2	F2	F1
6	Fumaric acid [d]	2 : 1	F1	F1	F1	Free	F1	–	F2	–	F2	–	–	F1
7	Citric acid [e]	1 : 1	C1	C1	C1	C1	C1	C1	C1	C1	C2	–	C1	C1
8	Citric acid [e]	2 : 1	C1	C1	C1	C1	–	Free	C2	–	C2	–	C1	C1
9	Succinic acid [f]	1 : 1	S1	S1	S1	S1	S1	S1	S1	S1	S1	S1	S1	S1
10	Succinic acid [f]	2 : 1	S1	S1	S1	S1	S1 Free	S1	S1	S1	S1	–	S1	S1
	TAM (free base) [g]	–	Free	Free	Free	Free	–	–	Free	Free	Free	–	–	–

Abbreviations used in the table; MeOH, methanol; EtOH, ethanol; IPA, isopropyl alcohol; MeCN, acetonitrile; EtOA, ethyl acetate; IPE, isopropyl ether; THF, tetrahydrofuran; DCM, dichloromethane; cHex, cyclohexane; TAM, tamoxifen; CA, counter acid.

[a] Raman spectra of crystals formed with TAM and methanesulfonic acid (1:1) were classified as M1 or M2.

[b] Raman spectra of crystals formed with TAM and benzenesulfonic acid (1:1) were classified as B1 or B2.

[c] Raman spectra of crystals formed with TAM and L-tartaric acid (1:1, 2:1) were same patterns and classified as T1, T2 or T3.

[d] Raman spectra of crystals formed with TAM and fumaric acid (1:1, 2:1) were same patterns and classified as F1 or F2.

[e] Raman spectra of crystals formed with TAM and citric acid (1:1, 2:1) were same patterns and classified as C1 or C2.

[f] Raman spectrum of crystals formed with TAM and succinic acid (1:1, 2:1) was just one pattern and classified as S1.

[g] Raman spectrum of TAM crystals was just one pattern and classified as Free.

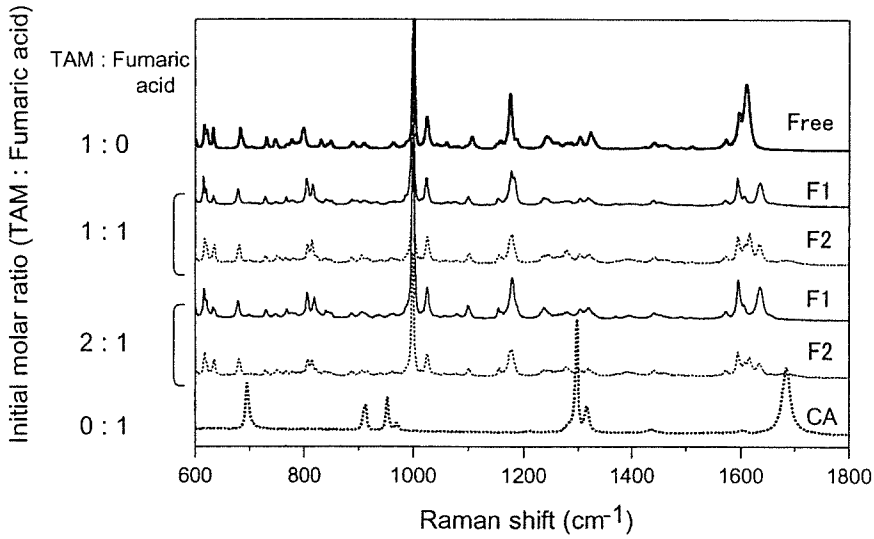

Fig. 2. Raman spectra of tamoxifen (TAM), TAM fumarate, and fumaric acid crystals. TAM fumarate was prepared with TAM and fumaric acid (1:1 and 2:1) on a 96-well plate. Free, F1, F2, and counter acids (CA) correspond to the classification in Table I. Heavy solid line (—), TAM (free); solid line (—), TAM fumarate (F1); dotted line (---), TAM fumarate (F2); and heavy dotted line (---), fumaric acid (CA).

RESULTS

Chemical Information from Salt Screening on 96-Well Plate

Polarizing light microscope observations indicated that 114 crystalline solids were obtained out of 132 wells on the 96-well plates. Except for amorphous or oily substances observed by PLM, crystals obtained were analyzed by Raman microscope. The results of Raman microscopy for tamoxifen salts on the 96-well plate are shown in Table I. The Raman spectra of all crystals were sorted in comparison with each pattern in the shift region 600–1800 cm^{-1}. Sorted spectra were compared with those of the tamoxifen free base and counter acids measured separately. Crystals from the free base and counter acids detected by Raman microscopy are hereafter denoted as free and CA, respectively. Crystalline forms in the binary mixtures of tamoxifen and acid on the plate identified as salts showing different spectra are presented numerically with initial, i.e., M1 and M2 for two crystalline forms of tamoxifen mesylate salt.

Raman spectra indicated that salt screening revealed that only one crystalline form was obtained for both tamoxifen free base and succinate salt, whereas two potential polymorphic forms were obtained for tamoxifen mesylate, besylate, fumarate, and citrate salts, and three potential polymorphic forms were obtained for tamoxifen L-tartrate salt, including hydrate or solvate. In addition to potential polymorph information, the same crystalline forms were detected on the wells in molar ratios of 1:1 and 2:1 (tamoxifen/polybasic acid).

Chemical identification of solids was also performed by Raman microscope. Tamoxifen free base was detected on the wells in a molar ratio of 2:1 (tamoxifen/L-tartaric acid) in

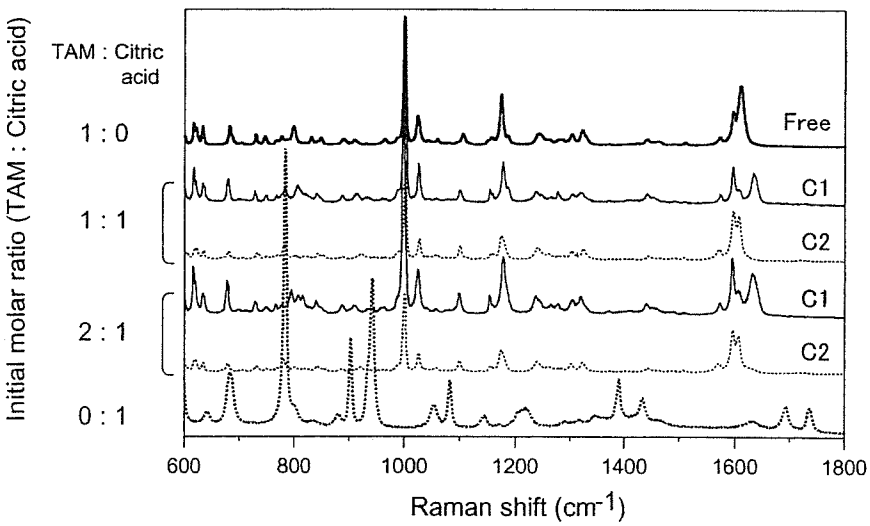

Fig. 3. Raman spectra of TAM, TAM citrate, and citric acid crystals. TAM citrate was prepared with TAM and citric acid (1:1 and 2:1) on a 96-well plate. Free, C1, and C2 correspond to the classification in Table I. Heavy solid line (—), TAM (free); solid line (—), TAM citrate (C1); dotted line (---), TAM citrate (C2); and heavy dotted line (---), citric acid.

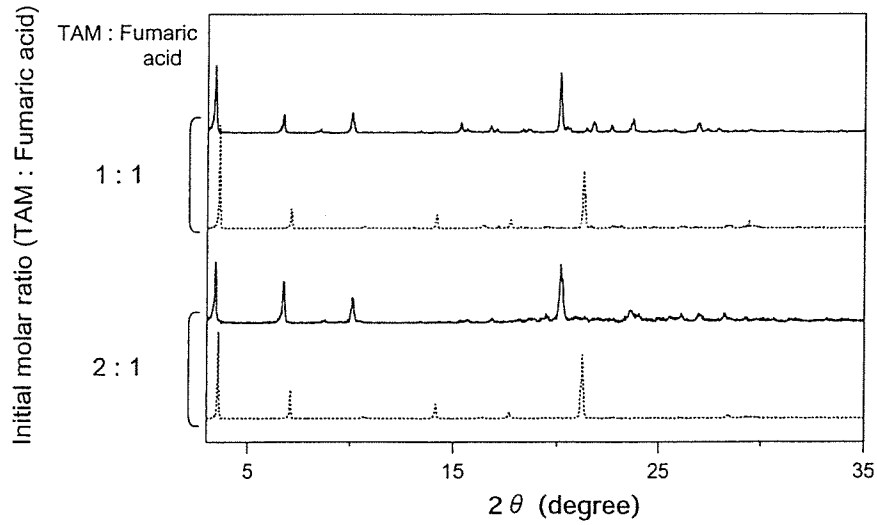

Fig. 4. Powder X-ray diffractometry (PXRD) patterns of TAM fumarate prepared with TAM and fumaric acid (1:1 and 2:1) on a large scale. Solid line (—), TAM fumarate form A; dotted line (----), TAM fumarate form B.

isopropyl alcohol, 2:1 (tamoxifen/L-tartaric acid) in isopropyl ether, 2:1 (tamoxifen/fumaric acid) in acetonitrile, 2:1 (tamoxifen/citric acid) in ethyl acetate, and 2:1 (tamoxifen/succinic acid) in acetone. Fumaric acid as a counter acid was detected in the well in a molar ratio of 1:1 (tamoxifen/fumaric acid) in toluene.

The Raman spectra of crystals in the wells with combinations of tamoxifen and fumaric acid are shown in Fig. 2. The Raman spectra of F1 in molar ratios of 1:1 and 2:1, as presented in Table I, showed the same patterns with distinct peaks at 1595 and 1638 cm^{-1}. The Raman spectra of F2 in molar ratios of 1:1 and 2:1 showed the same patterns with distinct peaks at 1596, 1618, and 1637 cm^{-1}. These results suggested that these crystals were identified as tamoxifen fumarate because their spectra were different from the spectra of either free base with a distinct peak at 1613 cm^{-1} or fumaric acid with the distinct peak at 1686 cm^{-1}.

The Raman spectra of the crystals in the wells with combinations of tamoxifen and citric acid are shown in Fig. 3. Raman spectra of C1 in molar ratios of 1:1 and 2:1, as presented in Table I, showed the same patterns with distinct peaks at 1595 and 1635 cm^{-1}. Raman spectra of C2 in molar ratios of 1:1 and 2:1 showed the same patterns with the distinct peaks at 1598 and 1608 cm^{-1}. These results suggested that these crystals were identified as tamoxifen citrate because their spectra were different from the spectra of either free base with a distinct peak at 1613 cm^{-1} or citric acid with distinct peaks at 1693 and 1735 cm^{-1}.

These results indicated that tamoxifen would prefer to form salts in a 1:1 molar ratio (tamoxifen/polybasic acid), and the excess amount of nonsalt-forming tamoxifen free base tended to be detected in the rows of the plate displaying a binary mixture of tamoxifen and polybasic acid in a molar ratio of 2:1.

Characterization of Salts by Scaled-Up Preparation

Tamoxifen fumarate and citrate prepared on a 300-mg scale were characterized using PXRD and ion chromatogra-

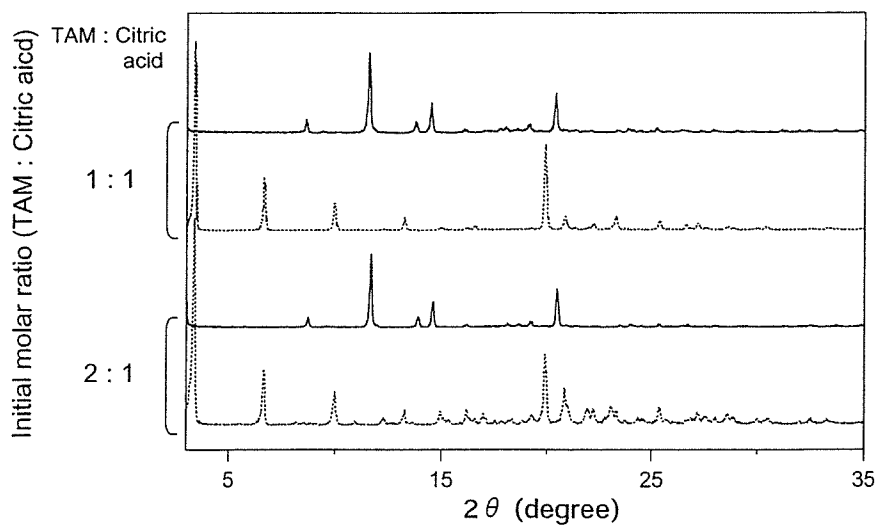

Fig. 5. PXRD patterns of TAM citrate prepared with TAM and citric acid (1:1 and 2:1) on a large scale. Solid line (—), TAM citrate form A; dotted line (----), TAM citrate form C.

phy. Tamoxifen fumarate prepared in molar ratios of 1:1 or 2:1 (tamoxifen/fumaric acid) was recrystallized in 12 solvents, and two crystalline forms were detected by PXRD in each preparation. PXRD patterns of these crystalline forms assigned as forms A and B, which were prepared in a 1:1 molar ratio, were confirmed to be the same as forms A and B prepared in a 2:1 molar ratio, respectively (Fig. 4). Ion chromatography indicated that the molar ratios of fumaric acid to tamoxifen free base were 1.02 and 1.03 for tamoxifen fumarate prepared in molar ratios of 1:1 and 2:1 (tamoxifen/fumaric acid), respectively. These results clearly suggested that crystals obtained were tamoxifen monofumarate.

Tamoxifen citrate was prepared in the same manner as tamoxifen fumarate, and at least two crystalline forms were detected by PXRD. Because forms A and B were the forms already reported (36), the new form was designated as form C. The PXRD patterns of the two crystalline forms assigned as forms B and C, which were prepared in a 1:1 molar ratio, were found to be the same as forms B and C prepared in a 2:1 molar ratio, respectively (Fig. 5). Ion chromatography indicated that the molar ratios of citric acid to tamoxifen were 1.01 and 0.99 for tamoxifen citrate prepared in molar ratios of 1:1 and 2:1 (tamoxifen/citric acid), respectively. These results suggested that the crystals obtained were tamoxifen monocitrate.

Characterization of the salts produced in the scaled-up preparation gave the same stoichiometrical information on tamoxifen fumarate and citrate salts as salt screening using the 96-well plates. These results suggested that salt screening with the 96-well plates would provide not only potential polymorph information but also prediction of stoichiometrical information on the salts.

DISCUSSION

We have first demonstrated that salt screening using multiwell plates and a Raman microscope can suggest stoichiometrical information on polyprotic salts. Salt screening using multiwell plates could be satisfactorily performed with less than 100 mg of drug candidate, and stoichiometrical information was easily obtained by comparing the Raman spectra of a drug candidate in the free base and counter acid condition, the free acid and counter base condition, and the salts found on the multiwell plates.

In the process of drug development, Raman microscopes have been widely used as an analytical tool for the chemical and physical identifications of either or both drugs and contaminants within pharmaceutical systems, which is also referred to as mapping of the dosage form (37,38). Physical indication, focusing on polymorph detected by Raman microscopy in place of PXRD, has been increasingly reported over the last few years (39). Attention has been also drawn to polymorphic evaluation by Raman microscopy of salt and polymorph screening of pharmaceutical drug molecules (22,24). However, to the best of our knowledge, chemical information obtained by Raman microscopy was not discussed.

In salt screening with Raman microscopy, it is possible to detect drug molecules, counter acids/bases, and salts individually. In salt formation of ionic drug molecules with polyprotic counterions, it is possible to form salt in more than one stoichiometric combination. Some ionic drug candidates form only one stoichiometric salt in combination with some polyprotic counterions, such as mono salt, and the other candidates form several combinations of salts, such as mono and hemi salts. In the crystalline form selection process, possible salts in various combinations should be prepared on a large scale and subsequently characterized because each combination of salt would show different physical properties (40). Therefore, it is important to obtain stoichiometrical information for efficient preparation of polyprotic salts.

The case that an ionic drug candidate formed only hemi salt with polyprotic counterion in salt screening has been previously reported (25). In the report, sertraline hemi-L-tartrate was obtained in 1:1 molar ratio (sertraline/L-tartaric acid); however, only polymorphism of salts was discussed, and stoichiometrical information of sertraline L-tartrate on multiwell plate was not fully elucidated (25). In this study, we performed tamoxifen salt screening on multiwell plate, and free base, counter acids, and salts could be identified by Raman microscope to obtain stoichiometrical information. Combining the information of Raman spectra of all crystals on multiwell plate, we could predict salt formation and stoichiometrical information of polybasic acid salts in addition to polymorph information. As the analytical tools for crystalline form selection, PXRD gives physical information and Raman microscopy provides both physical and chemical information. Physical information suggests the crystallinity and existence of polymorphism, whereas chemical information suggests salt formation and stoichiometrical combination of polyprotic salts. Therefore, Raman microscopy would be another useful analytical tool for salt screening, and further investigation for screening may be expected to expand.

In addition to salt screening for ionic drug candidates, cocrystals have been recently investigated as a pharmaceutical development option for neutral drug candidates (18,41). Cocrystals, categorized as multicomponent crystals such as solvate and salt, have the potential to improve drug candidate properties. Cocrystal preparations by melt crystallization, grinding, and recrystallization from solvents have been reported (11,41,42). Cocrystal screening could be performed with drug candidates and pharmaceutically acceptable excipients on multiwell plates. Cocrystal screening using Raman microscopes will also provide effective information for scaled-up preparation because there would be numerous stoichiometrical combinations with drug candidates and excipients.

In conclusion, our investigation enabled the successful development of salt screening methodology by using a Raman microscope, providing information on salt formation and stoichiometrical combinations of polyprotic salts, as well as polymorphism. Stoichiometrical information of polyprotic salts with small amount of drug candidate allows efficient crystalline form selection process by saving bulk.

ACKNOWLEDGMENTS

We wish to thank Prof. Makoto Otsuka, Research Institute of Pharmaceutical Sciences, Musashino University, and Dr. Naofumi Hashimoto, Pfizer Japan Inc. for their encouragement and valuable suggestions throughout this work.